Annals of Physics 412 (2020) 168022

Contents lists available at ScienceDirect

Annals of Physics

journal homepage: www.elsevier.com/locate/aop

Two-dimensional Klein tunneling for massive Dirac fermions with a defined helicity

Jorge Navarro-Giraldo [a,*], Carlos Quimbay [b]

[a] Central European Institute of Technology, CEITEC BUT, Purkyňova 656/123, 61200 Brno, Czech Republic

[b] Departamento de Física, Universidad Nacional de Colombia, Ciudad Universitaria, Bogotá, D. C., Colombia

ARTICLE INFO

Article history:
Received 15 August 2019
Accepted 29 October 2019
Available online 5 November 2019

Keywords:
Klein tunneling
Dirac equation
Tunnel junctions

ABSTRACT

The main goal of this work is to study the role played by the helicity in the two-dimensional Klein tunneling for massive Dirac fermions. To this end, we consider the cases in which massive Dirac fermions with a defined helicity are scattered by step and barrier electrostatic potentials. For each potential, we first calculate the contributions of fermion states with conserved and inverted helicity to the reflection and transmission coefficients, analyzing how the potential (V_0), fermion's mass, energy (E) and angle of incidence affect them. In the step potential case, we find that the transmission probability for fermion states with inverted helicity is small when $V_0 < E$, but becomes dominant when $V_0 > E$. In the barrier potential case, this probability is always null. This behavior is explained by the breaking of the helicity conservation by the mass term, allowing the reflection of states with inverted helicity in both potentials, and transmission of inverted helicity states only in the step potential. Finally, we give some insights on the consequences of our results in materials with Dirac-like quasiparticles, such as graphene, topological insulators and Weyl semimetals.

© 2019 Elsevier Inc. All rights reserved.

1. Introduction

When Klein, in 1929, studied the transmission of electrons through electrostatic potentials in the relativistic formalism of Dirac's equation, he found a non-negligible transmission probability even

* Corresponding author.
E-mail addresses: Jorge.Navarro@ceitec.vutbr.cz (J. Navarro-Giraldo), cjquimbayh@unal.edu.co (C. Quimbay).

https://doi.org/10.1016/j.aop.2019.168022
0003-4916/© 2019 Elsevier Inc. All rights reserved.

in the limit of very high potentials [1], in contrast to the exponentially suppressed transmission in non-relativistic quantum mechanics. The origin of this counterintuitive result, which is known as Klein paradox or Klein tunneling (KT), was explained by the presence of non-negative energy states inside the potentials [1,2]. However, it is very difficult to test this effect experimentally on free electrons. In order to observe KT, Bohr and Sauter formulated that a potential difference comparable to the electron's rest energy has to be achieved in a spatial length of the order of the electron's Compton wave length [3], yielding an electric field of the order of 10^{18} V/m [4,5]. This corresponds to Schwinger's limit of electron–positron pair creation [6], which is unattainable with the current technology.

On the other hand, the discovery of graphene opened the possibility of testing the KT in a condensed matter system [7]. In single-layer graphene, the charge carriers behave as massless spin 1/2 quasiparticles described by an effective Dirac's equation in (2+1) dimensions [8]. In this material, the experimental realization of step and barrier electrostatic potentials are p-n and n-p-n junctures, respectively, requiring electric fields of the order of 10^7 V/m to observe KT, routinely achieved in such systems [7]. In this context, KT manifests as the perfect transmission of normal-incident charge carriers through the juncture, independently of the barrier's spatial length or potential value, explained by the fact that the pseudospin is conserved in the transmission process [7]. Subsequently, KT in graphene was demonstrated experimentally by Young et al. [9] and Stander et al. [10], moreover, recent experimental studies on the transmission probability dependence upon the angle of incidence have been reported [11]. Furthermore, the observation of KT is expected in materials with Dirac-like quasiparticles, such as topological insulators and Weyl semimetals [12–15].

Nevertheless, KT is an undesirable effect in the design of graphene-based electronic components [16], most notably, it implies a difficulty to turn off a graphene-based transistor [10,16]. Hence, a way to limit the KT is necessary, and can be done by targeting the two related causes for the perfect transmission, namely, the massless nature of the charge carriers and the pseudospin conservation in the scattering process [7]. In graphene, the charge-carriers obtain a mass by opening a gap in the band structure, which can be achieved by breaking the inversion symmetry in graphene's A and B sublattices [17–19], or in other words, breaking the pseudospin symmetry. However, experimental evidence on how the band gap affects the behavior of reflected and transmitted particles with respect to their pseudospin degree of freedom is lacking. On the other hand, theoretical studies on two-dimensional KT for massive fermions are available [20–22], but only for the barrier potential the helicity contribution to the reflection and transmission coefficients is explicitly obtained [20], and, similarly as in the experimental case, it is not clear how the mass allows changes of helicity in the scattering process.

In this paper, we present the results of KT for spin 1/2 fermions with a given helicity state being scattered first by a step electrostatic potential and second by a barrier electrostatic potential, considering arbitrary angles of incidence. To perform the calculations, we use bispinors that are simultaneously eigenfunctions of Dirac's Hamiltonian and the helicity in each region defined by the potential, and considering continuity conditions on them we find the contribution of helicity conservation and helicity inversion to the reflection and transmission coefficients. In contrast to previous studies [20–26], we focus on the helicity role in the KT, studying how the potential, the fermion's mass, energy, and angle of incidence affect the reflection and transmission coefficients, and what is the contribution of the helicity inverted states on them. Our analysis is done considering the three energy zones (namely, the diffusion, evanescent and Klein zones) defined by the parameters of the problem [20], finding distinctive behavior in each of them. In the massless case, we find that helicity is conserved in the process, as expected. However, for massive fermions in both potentials, helicity inversion is present in the reflection probabilities, concluding that the mass term breaks the helicity conservation. Furthermore, when $V_0 > E$, helicity inverted states dominate the transmission in the step potential, but in the barrier potential we find that this contribution is completely absent in accordance with previous results [20,21].

At the end of the paper, we give some insights about the application of the present results in the transport properties of p-n and n-p-n junctures of gapped single-layer graphene and materials with massive Dirac-like quasiparticles. The interested reader may refer to Ref. [27], where we calculated the conductance in gapped single-layer graphene as a function of the charge carrier density and the band gap, considering incoming fermions with fixed (pseudo)helicity.

2. Formalism

In the single-particle formalism, a relativistic spin 1/2 fermion in 2+1 dimensions, under an external electrostatic potential, is described by the Dirac's Hamiltonian

$$H = c\boldsymbol{\sigma}\cdot\hat{\boldsymbol{p}} + \sigma_3 mc^2 + V(x), \tag{1}$$

where m is the fermion's mass, c is the speed of light, $\hat{\boldsymbol{p}} = (p_1, p_2)$ is the momentum operator, $V(x)$ is the electrostatic potential which in our problem depends only on the x coordinate, and $\boldsymbol{\sigma} = (\sigma_1, \sigma_2)$ and σ_3 are the Pauli matrices. In 2+1 dimensions, Dirac's Hamiltonian is represented by a 2×2 matrix with complex components having associated spinor wave functions, instead of the usual bispinors in 3+1 dimensions. However, the helicity operator $\hat{h} = \boldsymbol{\sigma}\cdot\hat{\boldsymbol{p}}/p$ no longer commutes with the Hamiltonian, losing the ability to label states by energy and helicity simultaneously. To overcome this difficulty, we work with a Hamiltonian with extended dimensionality (the same as in 3+1), which guarantees commutation with the helicity [28]:

$$H = c\boldsymbol{\alpha}\cdot\hat{\boldsymbol{p}} + \beta mc^2 + V(x). \tag{2}$$

The matrices $\boldsymbol{\alpha} = (\alpha_1, \alpha_2)$ and β are

$$\alpha_1 = \begin{pmatrix} 0 & \sigma_1 \\ \sigma_1 & 0 \end{pmatrix}, \quad \alpha_2 = \begin{pmatrix} 0 & \sigma_2 \\ \sigma_2 & 0 \end{pmatrix}, \quad \beta = \begin{pmatrix} \sigma_0 & 0 \\ 0 & -\sigma_0 \end{pmatrix}, \tag{3}$$

with σ_0 the identity matrix in 2×2 dimensions.

In graphene, the Hamiltonian describing the low energy excitations can be obtained from Eq. (2) by making $m = 0$, $V = 0$, replacing c by the Fermi velocity of the charge carriers v_F, and a rotation of the Hamiltonian is performed obtain a block-diagonal form [27]. In that case, instead of the spin, the Pauli matrices represent the two sublattices in graphene's crystal structure [7], referred as the pseudospin. From now on, we work with units $c = \hbar = 1$.

Since the potential only depends on x, the momentum in the y direction, p_2, is conserved, and the wave function for Dirac's Hamiltonian is

$$\Psi(x, y, t) = \psi(x)\, e^{i(yp_2 - Et)}. \tag{4}$$

Therefore, the wave function's dependence upon x, and eventually upon other degrees of freedom, is included in the term $\psi(x)$.

In the free case ($V(x) = 0$), the eigenvalues of Dirac's Hamiltonian represent the energy of a relativistic fermion

$$E = s\sqrt{p^2 + m^2}, \tag{5}$$

with p the magnitude of momentum, and the parameter $s = \text{sign}(E)$ representing a particle (antiparticle) state if $s = 1$ ($s = -1$). In the free case, the wave functions of Dirac's Hamiltonian are [28]

$$\psi_s(x) = N \begin{pmatrix} \chi \\ \frac{\boldsymbol{\sigma}\cdot\boldsymbol{p}}{E+m}\chi \end{pmatrix} e^{ixp_1}, \tag{6}$$

being χ a two-component column vector, N a normalization factor, and $\boldsymbol{p} = (p_1, p_2) = (p\cos\phi, p\sin\phi)$ the momentum's eigenvalue, with ϕ the direction of this vector measured from the x-axis. The subscript s indicates particle or antiparticle states depending on its value.

To further classify the wave functions, we use the helicity operator, defined as the projection of the spin in momentum's direction, $\hat{h} = \boldsymbol{\sigma}\cdot\hat{\boldsymbol{p}}/p$ [28]. In a 4×4 representation, it is given by $\hat{h}_4 = \text{diag}(\hat{h}, \hat{h})$. The helicity operator commutes with Dirac's Hamiltonian making it a good quantum number [28], whose eigenstates are

$$\chi^{\uparrow} = \begin{pmatrix} 1 \\ \frac{p_1 + ip_2}{p} \end{pmatrix}, \quad \chi^{\downarrow} = \begin{pmatrix} \frac{-p_1 + ip_2}{p} \\ 1 \end{pmatrix}, \tag{7}$$

where the index $\uparrow$ ($\downarrow$) denotes a helicity eigenstate with eigenvalue +1 (-1).

The eigenstates in Eq. (7) are the natural candidates to be the column vectors in the Hamiltonian's wave function in Eq. (6), nevertheless, it is important to state an additional consideration. Since the group velocity of the wave-packet is[1] $\boldsymbol{v}_{\text{group}} = \nabla_{\boldsymbol{p}} E = \boldsymbol{p}/(s|E|)$, which depends on the particle/antiparticle parameter s, the direction of movement of antiparticles is opposite to their momentum [1]. Therefore, if antiparticles must move in the same direction as particles (as in the problem we consider later), then their momentum must be modified to $\boldsymbol{p} = (-p\cos\phi,\ -p\sin\phi)$ [1,4]. In general, the linear momentum of a fermion is $\boldsymbol{p} = (sp\cos\phi,\ sp\sin\phi)$, valid for both particles and antiparticles. This changes the helicity eigenstates to

$$\chi^{\uparrow} = \begin{pmatrix} 1 \\ se^{i\phi} \end{pmatrix}, \quad \chi^{\downarrow} = \begin{pmatrix} -se^{-i\phi} \\ 1 \end{pmatrix}. \tag{8}$$

Inserting them in Eq. (6), we obtain the final form of Dirac's wave functions,

$$\psi_s^{\uparrow}(x) = N \begin{pmatrix} 1 \\ se^{i\phi} \\ P \\ sPe^{i\phi} \end{pmatrix} e^{ixp_1}, \tag{9}$$

$$\psi_s^{\downarrow}(x) = N \begin{pmatrix} -se^{-i\phi} \\ 1 \\ sPe^{-i\phi} \\ -P \end{pmatrix} e^{ixp_1}, \tag{10}$$

where the adimensional factor P was defined as

$$P = \frac{p}{E+m}. \tag{11}$$

Again, the index $\uparrow$ or $\downarrow$ is associated to the eigenstates of helicity, such that $\hat{h}_4\psi^{\uparrow} = \psi^{\uparrow}$, and $\hat{h}_4\psi^{\downarrow} = -\psi^{\downarrow}$. In Ref. [27] we used a slightly modified version of Eqs. (9) and (10), in such a way that the helicity eigenvalue depends on the parameter s in the following way: $\hat{h}_4\psi_s^{\uparrow} = s\psi_s^{\uparrow}$, and $\hat{h}_4\psi_s^{\downarrow} = -s\psi_s^{\downarrow}$. Therefore, in that study $\psi_s^{\uparrow}$ ($\psi_s^{\downarrow}$) has a negative (positive) helicity if antiparticle states are considered, on the contrary as in the present work.

If the potential now takes a constant value $V(x) = V_0$, Dirac's equation changes according to Eq. (2). The energy of the fermion now takes the value

$$E - V_0 = s'\sqrt{q^2 + m^2}, \tag{12}$$

where $s' = \text{sign}(E - V_0)$, and q is the new magnitude of the fermion's momentum. The wave functions can be obtained from Eqs. (9) and (10), by doing the following changes

$$\begin{aligned} E \to E - V_0, \quad s \to s' \\ \mathbf{p} \to \mathbf{q}, \quad \phi \to \theta \\ P \to Q \end{aligned} \tag{13}$$

where $\boldsymbol{q} = (q_1, q_2) = (s'q\cos\theta, s'q\sin\theta)$ is the fermion's linear momentum, θ the angle of the momentum relative to the x axis, and Q is defined as

$$Q = \frac{q}{E - V_0 + m}. \tag{14}$$

For fermions in a constant electrostatic potential, s' corresponds to the particle/antiparticle parameter. In this sense, if the potential energy V_0 is greater than the fermion's energy E, it is in an antiparticle state.

[1] Here, $\nabla_{\boldsymbol{p}} = \left(\frac{\partial}{\partial p_1}, \frac{\partial}{\partial p_2}\right)$.

3. Step potential

Now, we study the scattering of fermions through a step potential, of the form

$$V(x) = \begin{cases} 0, & \text{if } x < 0 \text{ (Region I)}, \\ V_0, & \text{if } x \geq 0 \text{ (Region II)}. \end{cases} \tag{15}$$

Defining $x < 0$ as the region I, and $x \geq 0$ as the region II.

We assume that the incoming fermions from region I are helicity-polarized, with positive helicity without loss of generality. The incident wave function takes the form of Eq. (9), with a normalization factor[2] $N = 1$.

Given that the potential only depends on x, the momentum p_2 is conserved in all regions [21], implying that only the $\psi(x)$ term of the wave function $\Psi(x, y, t)$ changes throughout the space. Also, as a result of the interaction with the potential, the reflected fermions at $x = 0$ may get an inversion in their helicity degree of freedom, which must be taken into account by means of the corresponding wave function. Therefore, the wave function in region I is constructed as a superposition of the incident wave function, and the reflected ones with positive and negative helicity, as follows,

$$\begin{aligned} \psi_{\mathrm{I}}(x) &= \psi_i + \psi_r + \psi_{r'} \\ &= \begin{pmatrix} 1 \\ se^{i\phi} \\ P \\ sPe^{i\phi} \end{pmatrix} e^{ixp_1} + \left[r \begin{pmatrix} 1 \\ -se^{-i\phi} \\ P \\ -sPe^{-i\phi} \end{pmatrix} + r' \begin{pmatrix} se^{i\phi} \\ 1 \\ -sPe^{i\phi} \\ -P \end{pmatrix} \right] e^{-ixp_1}, \end{aligned}$$

where ψ_i is the incident wave, ψ_r ($\psi_{r'}$) is the reflected wave function with positive (negative) helicity, and r (r') the reflection probability amplitude for positive (negative) helicity. The reflected wave functions were found from Eqs. (9) and ((10)) by changing the sign of p_1 [20,21], or equivalently, by changing the angle from ϕ to $\pi - \phi$.

The transmitted fermions at $x = 0$ are represented also as a superposition of both helicity states, however, since at $x \geq 0$ the potential takes the value V_0, we must consider the changes in the wave functions mentioned in Eq. (13). The wave function in region II is

$$\begin{aligned} \psi_{\mathrm{II}}(x) &= \psi_t + \psi_{t'} \\ &= \left[t \begin{pmatrix} 1 \\ s'e^{i\theta} \\ Q \\ s'Qe^{i\theta} \end{pmatrix} + t' \begin{pmatrix} -s'e^{-i\theta} \\ 1 \\ s'Qe^{-i\theta} \\ -Q \end{pmatrix} \right] e^{ixq_1}, \end{aligned} \tag{16}$$

with ψ_t ($\psi_{t'}$) the transmitted wave function with positive (negative) helicity, and t (t') the transmission probability amplitude for helicity conservation (inversion).

To find a relation between ϕ and θ, it is considered the conservation of the p_2 component of the momentum, yielding a Snell law for the fermion's in this system [21]

$$\begin{aligned} p_2 &= q_2 \\ sp \sin\phi &= s'q \sin\theta. \end{aligned} \tag{17}$$

It is observed that if s and s' have different values, meaning that the scattering is between particles on one hand, and antiparticles on the other hand, the "refraction index" yields a negative value, in the same way as Veselago lenses in electrodynamics [29] and charge carrier lensing in graphene [30].

The reflection and transmission amplitudes are found by imposing continuity conditions at $x = 0$, such that $\psi_{\mathrm{I}}(x = 0) = \psi_{\mathrm{II}}(x = 0)$. This leads to the following linear system of equations in matrix

[2] Since we are interested in the reflection and transmission coefficients, which are relative quantities with respect to the amplitude of the incident wave function, then N can take an arbitrary value.

form

$$\begin{pmatrix} 1 & se^{i\phi} & -1 & s'e^{-i\theta} \\ -se^{-i\phi} & 1 & -s'e^{i\theta} & -1 \\ P & -sPe^{i\phi} & -Q & -s'Qe^{-i\theta} \\ -sPe^{-i\phi} & -P & -s'Qe^{i\theta} & Q \end{pmatrix} \begin{pmatrix} r \\ r' \\ t \\ t' \end{pmatrix} = \begin{pmatrix} -1 \\ -se^{i\phi} \\ -P \\ -sPe^{i\phi} \end{pmatrix}.$$

It is straightforward to solve this system, obtaining the following results for the probability amplitudes

$$r = \frac{ie^{i\phi}\left[(P^2+Q^2)\sin\phi - 2ss'PQ\sin\theta\right]}{P^2+Q^2+2ss'PQ\cos(\phi+\theta)}, \tag{18}$$

$$r' = \frac{s(P^2-Q^2)\cos\phi}{P^2+Q^2+2ss'PQ\cos(\phi+\theta)}, \tag{19}$$

$$t = \frac{(P^2+PQ)\cos\phi\,(e^{i\phi}+ss'e^{-i\theta})}{P^2+Q^2+2ss'PQ\cos(\phi+\theta)}, \tag{20}$$

$$t' = \frac{s(P^2-PQ)\cos\phi\,(1-ss'e^{i(\phi+\theta)})}{P^2+Q^2+2ss'PQ\cos(\phi+\theta)}. \tag{21}$$

To find the reflection and transmission coefficients, we must consider the probability density current $\boldsymbol{j}$, and the fact that its normal component with respect to the potential interface (i.e. the vertical line $x = 0$) must be conserved. The probability density current is defined as $\boldsymbol{j} = (j_1, j_2) = (\Psi^\dagger\alpha_1\Psi,\ \Psi^\dagger\alpha_2\Psi)$. Therefore, the conservation of the x component of $\boldsymbol{j}$ leads to

$$j_{i,1} + j_{r,1} + j_{r',1} = j_{t,1} + j_{t',1} \tag{22}$$

or equivalently,

$$-\frac{j_{r,1}}{j_{i,1}} - \frac{j_{r',1}}{j_{i,1}} + \frac{j_{t,1}}{j_{i,1}} + \frac{j_{t',1}}{j_{i,1}} = 1 \tag{23}$$

where $j_{i,1} = \Psi_i^\dagger\alpha_1\Psi_i$ is the probability current density associated to the incident wave function $\Psi_i(x,y,t) = \psi_i(x)e^{i(p_2y-Et)}$, and $\psi_i(x)$ was defined implicitly in Eq. (16). Similar equations for the reflected current densities $j_{r,1}$ and $j_{r',1}$, and the transmitted current densities $j_{t,1}$ and $j_{t',1}$ hold. Eq. (23) defines the transmission and reflection coefficients as

$$R = \left|-\frac{\Psi_r^\dagger\alpha_1\Psi_r}{\Psi_i^\dagger\alpha_1\Psi_i}\right|, \quad R' = \left|-\frac{\Psi_{r'}^\dagger\alpha_1\Psi_{r'}}{\Psi_i^\dagger\alpha_1\Psi_i}\right|, \tag{24}$$

$$T = \left|\frac{\Psi_t^\dagger\alpha_1\Psi_t}{\Psi_i^\dagger\alpha_1\Psi_i}\right|, \quad T' = \left|\frac{\Psi_{t'}^\dagger\alpha_1\Psi_{t'}}{\Psi_i^\dagger\alpha_1\Psi_i}\right|. \tag{25}$$

From them, it is straightforward to obtain the following results

$$\begin{aligned} &R = |r|^2, \quad R' = |r'|^2, \\ &T = \left|\mathrm{Re}\left(\frac{Q\cos\theta}{P\cos\phi}\right)\right| |t|^2, \quad T' = \left|\mathrm{Re}\left(\frac{Q\cos\theta}{P\cos\phi}\right)\right| |t'|^2, \end{aligned} \tag{26}$$

with Re the real part of the argument. The real part of the term is added *ad hoc* in the calculations, because otherwise, in the case when Q is imaginary, the probability conservation $R+R'+T+T' = 1$ is violated.

Some conclusions can be obtained from the reflection and transmission coefficients. First, it is observed that in a general scenario, helicity inversion is present in both transmission and reflection probabilities. One of our objectives is to study the extent of the contributions of helicity inversion in both reflection and transmission, and what is the role of fermion's mass on it. On the other hand, by definition the reflection and transmission coefficients conserve the probability:

$$R + R' + T + T' = 1. \tag{27}$$

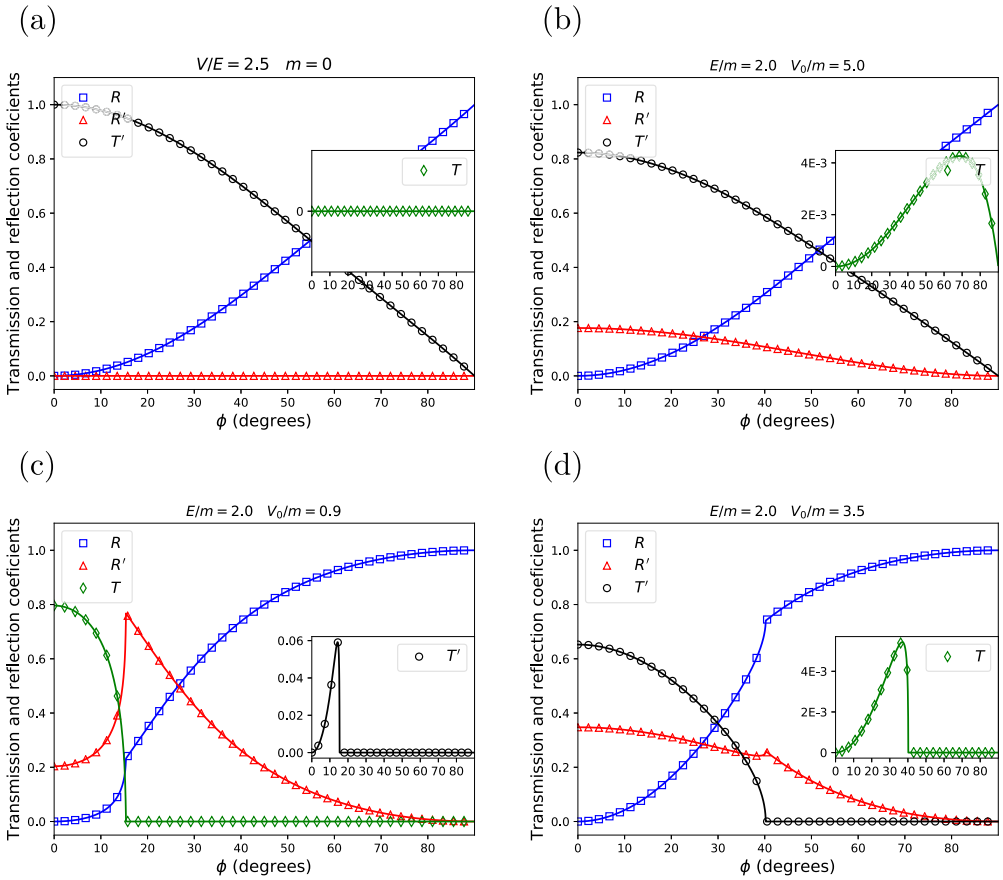

Fig. 1. Behavior of R, R', T y T' as a function of the incidence angle ϕ, for several values of potential V_0 and energy E, normalized to the fermion's mass m. (a) Massless case in the Klein zone, with $V_0/E = 2.5$. The reflection (transmission) is entirely by states with conserved (inverted) helicity. (b) Similar as before, but with massive fermions, such that $V_0/E = 2.5$ and $E/m = 2.0$. R' and T are non-zero, but T' dominates over T. Since $V_0 > 2E$ no angles of total reflection are observed. (c) $E/m = 2.0$ and $V_0/m = 0.9$, thus the diffusion and evanescent energy zones are shown. The presence of angles of total reflection marks the transition form the diffusion to the evanescent zone, with a critical angle $\phi_{crit} = 15.34°$ calculated from Eq. (28). There is transmission probability for helicity inversion states (T'), but it is small compared to T. (d) Klein and evanescent zones, with $E/m = 2.0$ and $V_0/m = 3.5$. Since $V_0 < 2E$, a transition from the Klein to the evanescent zone is present at an angle $\phi_{crit} = 40.2°$. The transmission probability for inverted helicity states is dominant over T.

As a consistency check, we examine the normal incidence case, $\phi = 0$. In this case, we have

$$R = 0, \quad R' = \left| \frac{P^2 - Q^2}{(P + ss'Q)^2} \right|^2$$

$$T = \frac{|PQ||P+Q|^2\,|1+ss'|}{|P+ss'Q|^2}, \quad T' = \frac{|PQ|\,|P-Q|^2\,\left|1-ss'\right|}{|P+ss'Q|^2}.$$

The result $R = 0$ means that for head-on collisions, the reflected fermions can only present inverted helicity when compared to the incident ones [20]. In graphene and Dirac materials with massless charge carriers, this has a more profound implication. In this context, $m = 0$ implies that the dimensionless parameters take the values $P = s$ and $Q = s'$, where s and s' now represent the conduction/valence bands in each spatial region rather than particles/antiparticles.

The helicity is replaced with the pseudospin in graphene, or with chirality in Dirac materials [31]. It is straightforward to prove that $R' = 0$, and either T or T' is zero, depending on the value ss'. For instance, if $0 < E < V_0$, then $ss' = -1$, implying that $T = 0$ and $T' = 1$, regardless of the energy and potential values, meaning that total transmission is always expected for head-on collisions [7]. Total transmission at normal incidence is the manifestation of Klein tunneling in graphene and Dirac materials, and as can be observed, it is a consequence of the helicity conservation in the reflection process (or equivalently, the restriction of reflection with inverted helicity). In graphene, this translates into conservation of pseudospin, [7], and the conservation of chirality in topological insulators [31].

In fact, for $m = 0$, the helicity conservation in the reflected fermions is not only manifested at normal incidence, but for arbitrary angles of incidence as well. Since in the massless case $P = s$ and $Q = s'$, the term $P^2 - Q^2$ in the numerator of r' is equal to zero, implying $r' = 0$ for massless particles. Additionally, either T or T' are null depending on the values of E and V_0, specifically, $T = 0$ if $E < V_0$, or $T' = 0$ if $E > V_0$. Fig. 1(a) shows this situation in the case $V_0 > E$, where the transmission is entirely through inverted helicity states.

Now, we analyze the transmission and reflection coefficients as a function of E, V_0, and arbitrary angles of incidence ϕ. The analysis is done in the different energy zones as defined in [20], namely,

$$V_0 < E - \sqrt{m^2 + p_2^2} \quad \text{(diffusion zone)}$$
$$E - \sqrt{m^2 + p_2^2} \leq V_0 \leq E + \sqrt{m^2 + p_2^2} \quad \text{(evanescent zone)}$$
$$E + \sqrt{m^2 + p_2^2} < V_0 \quad \text{(Klein zone)}$$

They are defined considering the momentum $q_1 = \sqrt{(E - V_0)^2 - m^2 - p_2^2}$, and evaluating the values at which it is real or imaginary. For instance, in the diffusion and Klein zones, q_1 is real, and therefore, plane wave solutions for the wave function in region II are valid, while in the evanescent zone,[3] q_1 is imaginary, implying that the transmission in region II is through evanescent waves. In the diffusion zone, the transmitted states in the potential region are particles, whereas in the Klein zone they are antiparticles.

Fig. 1(a) shows the behavior of the reflection and transmission coefficients in the Klein energy zone, in the case $m = 0$. As already mentioned, the reflection (transmission) is entirely through conserved (inverted) helicity states. However, this situation changes for massive fermions. Fig. 1(b) is similar as the previous one, in the sense that the ratio V_0/E is the same, but now the mass is different to zero. At normal incidence, the transmission gets reduced by the reflection through states with inverted helicity. Additionally, although the transmission coefficient for states with conserved helicity is non-zero, it is around two orders of magnitude lower than T'. This is a consistent trend: T' is dominant over T when $V_0 > E$, but T dominates over T' when $V_0 < E$.

In Fig. 1(c), the energy and potential take the values $E/m = 2$ and $V_0/m = 0.9$, such that the case of diffusion and evanescent zones is shown. In this situation, the transmission coefficients are equal to zero from a certain angle ϕ. This happens because as ϕ increases, the value of p_2^2 increases as well ($p_2 = sp \sin\phi$), taking the system from the diffusion zone to the evanescent zone. This can be seen more clearly if we consider the normal incidence case $p_2 = 0$, where the condition for the diffusion zone $V_0/m < E/m - \sqrt{1 + p_2^2/m^2}$ is met. Increasing ϕ lowers the value at the right hand side of the inequality, taking the system to the evanescent zone after some critical value of ϕ, found to be

$$\phi_{crit} = \sin^{-1} \sqrt{\frac{(E - V_0)^2 - m^2}{E^2 - m^2}}, \tag{28}$$

[3] In Ref. [20] this zone is denoted as the "tunneling zone", however, as we will show, there is no tunneling here in the potential step or the potential barrier.

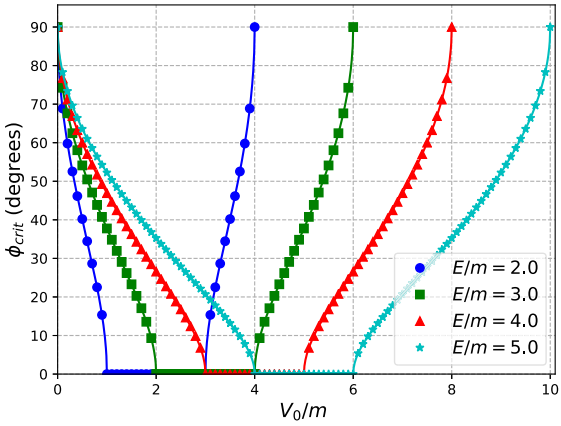

Fig. 2. Behavior of ϕ_{crit} as a function of the potential V_0/m, for several values of E/m. If the condition $E-m < V_0 < E+m$ holds, then $\phi_{crit} = 0$ implying total reflection for all angles of incidence. In that situation, the system is always in the evanescent energy zone. On the contrary, if $V_0 > 2E$ then no critical angles are found, therefore total reflection is absent. $E/m = 2.0$ corresponds to the case shown in Fig. 1(b)–(d).

obtained by finding the values of p_2 that turn q_1 into an imaginary quantity. Focusing our analysis in the diffusion zone, it is noticed that for low angles, T and R' are the dominant terms, however, as the angle increases, R starts to play a role in the total reflection. The transmission with inverted helicity, T', is found to be small compared to T, being only comparable to it in the case of angles close to ϕ_{crit}, where T is dropping to zero. On the other hand, for large incidence angles the reflection is dominated by R, while R' drops to zero. This behavior is consistent in all energy zones. Finally, the fact that the transmission coefficients T and T' are zero in the evanescent energy zone, along with the probability conservation condition, implies that $R + R' = 1$.

Fig. 1(d) depicts a transition from the Klein to the evanescent zone. Here, q_1 goes from being real to imaginary, where the critical angle is still ϕ_{crit} given in Eq. (28). In this situation T' dominates over T, as mentioned.

The behavior of the critical angle ϕ_{crit} of total reflection as a function of V_0 is shown in Fig. 2. It can be noticed that for the considered energies, there exists a range of V_0 values at which ϕ_{crit} is zero, implying that the system is in the evanescent energy zone for all angles of incidence, and total reflection is always expected. This situation is observed if the condition $E-m < V_0 < E+m$ is met. Additionally, no angles of total reflection are observed if $V_0 > 2E$, as it is the case of Fig. 1(a) and (b).

A more clear dependence of the transmission coefficients upon the mass is shown in Fig. 3(a)–(d). In those graphs, T and T' are plotted as a function of both V_0/E and m, for a fixed ϕ. Fig. 3(a) and (b) represent the transmission coefficient T at angles of incidence $\phi = 0$ and $\phi = 20°$, respectively. In both cases, it can be observed that T is only dominant if $V_0 < E$, and that a region of no transmission around $V_0/E = 1$ is present in Fig. 3(b), compared to Fig. 3(a). This is a result of finding the system in the evanescent energy zone, in close relation to the critical angle argument discussed previously. Fig. 3(c) and (d) show a similar situation for T', noticing that it is only relevant if $V_0 > E$. The appearance of greenish colors instead of yellow in Fig. 3(d), corresponding to $\phi = 20°$, implies a lower transmission probability compared to normal incidence. Again, no transmission around $V_0/E = 1$ is an indication that the system is in the evanescent zone, however, if $V_0/E > 2$ no transition to the evanescent zone is present, implying that T' is non-null for all mass values. Negative values of V_0 were included, such that the electrostatic potential is now attractive for positive-charged fermions, that is, the barrier potential changes to a potential well.

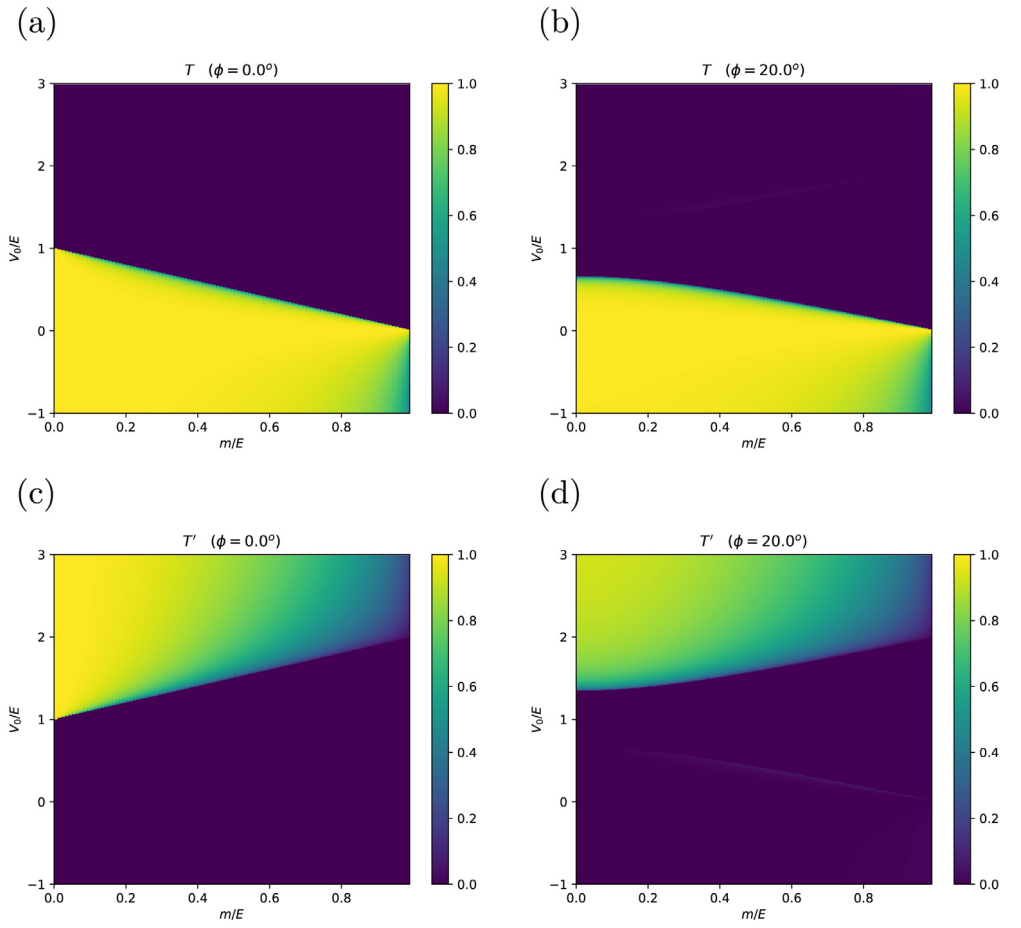

Fig. 3. Behavior of T and T' for fixed ϕ, as a function of m/E and V_0/E. High to low transmission are plotted in yellow-ish to green-ish colors, respectively, while zero transmission is in dark blue. (a) Transmission coefficient for conserved helicity states T at normal incidence, $\phi = 0$. Notice that it is relevant only when $V_0 < E$. (b) Transmission coefficient T at $\phi = 20°$. For small mass, zero transmission is obtained around $V_0/E = 1$ compared to the previous case, in accordance to the critical angle condition marking the transition to the evanescent zone. (c) Transmission probability for inverted helicity states at normal incidence, $\phi = 0$. On the contrary to Fig. (a), T' is dominant when $V_0 > E$. For a fixed V_0, it can be observed that the transmission coefficient decreases as m increases. (d) Transmission coefficient T' at $\phi = 20°$. Green colors instead of yellow in the graph imply a lower value of T', compared to the case of normal incidence. Negative potential values were included, meaning that the electrostatic potential is attractive (potential well) for the incoming fermions. (For interpretation of the references to color in this figure legend, the reader is referred to the web version of this article.)

As a closing remark, we study the case $V_0 \gg E$. Under this condition, it follows that $Q \approx -1$ and $\theta \approx 0$, from which it is obtained

$$R_{V_0 \gg E} = \left| \frac{(P^2+1)\sin\phi}{P^2+1+2sP\cos\phi} \right|^2 \tag{29}$$

$$R'_{V_0 \gg E} = \left| \frac{(P^2-1)\cos\phi}{P^2+1+2sP\cos\phi} \right|^2 \tag{30}$$

$$T_{V_0\gg E} = \left| \frac{(P+1)(1-se^{i\phi})}{P^2+1+2sP\cos\phi} \right|^2 \tag{31}$$

$$T'_{V_0\gg E} = \left| \frac{(P-1)(1+se^{i\phi})}{P^2+1+2sP\cos\phi} \right|^2 \tag{32}$$

The non-null transmission of fermions through very high potentials was the original version of the Klein tunneling for free relativistic fermions, proposed in 1929 by Klein [1].

4. Barrier potential

Now we study the scattering of fermions on a barrier potential of spatial length L. The results and methods shown in the following paragraphs are equivalent to those found by De Leo and Rotelli in Refs. [20,21]. However, we introduce useful notation, generalization for antiparticle states via the parameters s and s', and further analysis which we believe will contribute to the literature of the field.

The potential has the following form

$$V(x) = \begin{cases} 0, & \text{if } x < 0 \text{ (Region I)} \\ V_0, & \text{if } 0 \le x \le L \text{ (Region II)} \\ 0, & \text{if } L < x \text{ (Region III)}. \end{cases} \tag{33}$$

As in the step potential, we consider helicity-polarized fermions incoming from region I, with positive helicity without loss of generality, and helicity inversion is permitted in the transmitted and reflected fermions.

In region I, the wave function is a superposition of the incident wave and the reflected ones with conserved and inverted helicity, such that it is given by Eq. (16). In region II, the wave function is superposition of the transmitted waves at $x = 0$, and the reflected ones at $x = L$

$$\psi_{\rm II}(x) = \left[a \begin{pmatrix} 1 \\ s'e^{i\theta} \\ Q \\ s'Qe^{i\theta} \end{pmatrix} + a' \begin{pmatrix} -s'e^{-i\theta} \\ 1 \\ s'Q^{i\theta} \\ -Q \end{pmatrix} \right] e^{ixq_1} + \left[b \begin{pmatrix} 1 \\ -s'e^{-i\theta} \\ Q \\ -s'Qe^{-i\theta} \end{pmatrix} + b' \begin{pmatrix} s'e^{i\theta} \\ 1 \\ -s'Qe^{-i\theta} \\ -Q \end{pmatrix} \right] e^{-ixq_1}. \tag{34}$$

Where a (a') is the transmission amplitude at $x = 0$ for positive (negative) helicity states, and b (b') is the reflection amplitude at $x = L$ for positive (negative) helicity states.

Finally, the wave function in region III is the superposition of waves with both helicity states

$$\psi_{\rm III}(x) = \left[t \begin{pmatrix} 1 \\ se^{i\phi} \\ P \\ sPe^{i\phi} \end{pmatrix} + t' \begin{pmatrix} -se^{-i\phi} \\ 1 \\ sPe^{-i\phi} \\ -P \end{pmatrix} \right] e^{ixp_1}. \tag{35}$$

The transmission and reflection amplitudes are found by solving the linear system of equations resulting from the continuity conditions $\psi_{\rm I}(x = 0) = \psi_{\rm II}(x = 0)$, and $\psi_{\rm II}(x = L) = \psi_{\rm III}(x = L)$. Defining $\alpha = spL\cos\phi$ and $\beta = s'qL\cos\theta$, the following equations are obtained

$$U \begin{pmatrix} 1 \\ r \\ r' \end{pmatrix} = M_1 \begin{pmatrix} a \\ a' \\ b \\ b' \end{pmatrix} \tag{36}$$

$$M_2 \begin{pmatrix} a \\ a' \\ b \\ b' \end{pmatrix} = V \begin{pmatrix} t \\ t' \end{pmatrix} \tag{37}$$

with

$$U = \begin{pmatrix} 1 & 1 & se^{i\phi} \\ se^{i\phi} & -se^{-i\phi} & 1 \\ P & P & -sPe^{i\phi} \\ sPe^{i\phi} & -sPe^{-i\phi} & -P \end{pmatrix}, \tag{38}$$

$$M_1 = \begin{pmatrix} 1 & -s'e^{-i\theta} & 1 & s'e^{i\theta} \\ s'e^{i\theta} & 1 & -s'e^{-i\theta} & 1 \\ Q & s'Qe^{-i\theta} & Q & -s'Qe^{i\theta} \\ s'Qe^{i\theta} & -Q & -s'Qe^{-i\theta} & -Q \end{pmatrix}, \tag{39}$$

$$M_2 = M_1 \begin{pmatrix} e^{i\beta} & 0 & 0 & 0 \\ 0 & e^{i\beta} & 0 & 0 \\ 0 & 0 & e^{-i\beta} & 0 \\ 0 & 0 & 0 & e^{-i\beta} \end{pmatrix}, \tag{40}$$

$$V = e^{i\alpha} \begin{pmatrix} 1 & -se^{-i\phi} \\ se^{i\phi} & 1 \\ P & sPe^{-i\phi} \\ sPe^{i\phi} & -P \end{pmatrix}. \tag{41}$$

The Appendix shows briefly how to solve them. The resulting transmission and reflection amplitudes are

$$r = \frac{-e^{i\phi}\sin\beta\,[(P^2+Q^2)\sin\phi - 2ss'PQ\sin\theta]}{f}, \tag{42}$$

$$r' = \frac{is\sin\beta\cos\phi(P^2-Q^2)}{f}, \tag{43}$$

$$t = \frac{2ss'PQ\,e^{-i\alpha}\cos\phi\cos\theta}{f}, \tag{44}$$

$$t' = 0, \tag{45}$$

with

$$f = (P^2+Q^2)i\sin\beta - ss'PQ[e^{i\beta}\cos(\theta-\phi) + e^{-i\beta}\cos(\theta+\phi)]. \tag{46}$$

In the barrier potential, the squared norm of the probability amplitudes does yield the correct reflection and transmission coefficients, as can be proven by applying the definitions in Eqs. (24) and (25) to the corresponding wave functions of this problem. Therefore, the reflection and transmission coefficients yield

$$R = \frac{\sin^2\beta\,|(P^2+Q^2)\sin\phi - 2ss'PQ\sin\theta|^2}{|f|^2} \tag{47}$$

$$R' = \frac{\sin^2\beta\cos^2\phi|P^2-Q^2|^2}{|f|^2}, \tag{48}$$

$$T = \frac{4\cos^2\phi\cos^2\theta|PQ|^2}{|f|^2}, \tag{49}$$

$$T' = 0. \tag{50}$$

Few remarks must be mentioned in regard to this result. First, the transmission coefficient for helicity inverted fermions is always zero, regardless of the incidence angle of the incoming fermions or other parameters, as was obtained by De Leo and Rotelli in [20,21]. This can be contrasted with the result for the step potential, where it was observed that when $V_0 > E$, the transmission is dominated by states with inverted helicity. It is expected that the transmission of helicity inverted states exist inside the barrier, however, the consequence outside it is the suppression of such states.

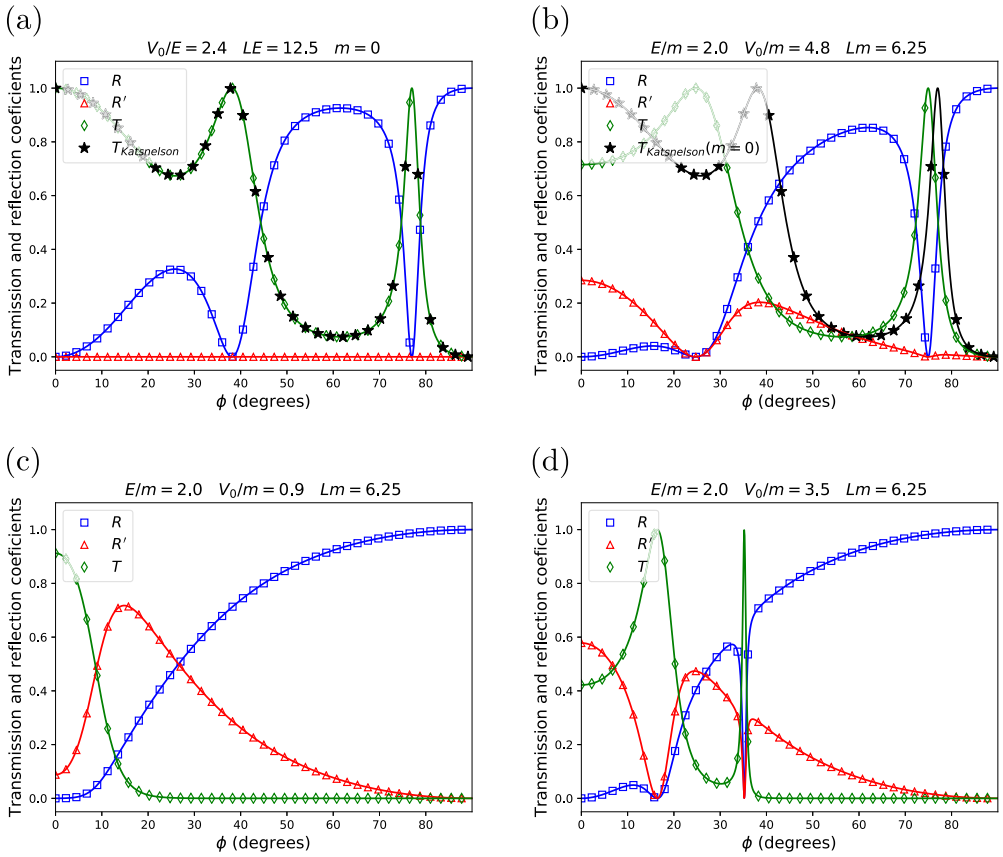

Fig. 4. Behavior of R, R', and T as a function of the incidence angle, for several values of E, V_0, L and m. (a) Massless case $m = 0$, with values of V_0 and L normalized with respect to the energy E. In this case, the reflection probability for helicity inverted states, R', is always zero, and total transmission is expected at normal incidence ($\phi = 0$). Our results correspond to the reported by Katsnelson et al. in Ref. [7] for pristine graphene, using the natural units $\hbar = v = 1$, being v the Fermi velocity. The remaining figures represent the massive case, with E, V_0 and L being normalized with respect to m. (b) Similar situation as before but with massive fermions, in the sense that V_0/E and LE have the same values as in Fig. 4(a). Now, the reflection probability R' is non-zero, and T is suppressed at normal incidence. For comparison, T for $m = 0$ is plotted. (c) The system is initially in the diffusion zone, as the condition $V_0 < E - \sqrt{m^2 + p_2^2}$ is met. The transition to the evanescent zone is evident by the suppression of T at some values of ϕ. (d) The system is initially in the Klein zone $V_0 > E + \sqrt{m^2 + p_2^2}$ and again, the transition the evanescent zone is observed by the suppression of T.

Second, by considering Eqs. (24) and (25), along with Eq. (22), the probability conservation condition $R + R' + T = 1$ holds true by definition.

Another consequence is that, as a result of the $\sin\beta$ dependence in the reflection coefficients, total transmission is present when $\beta = n\pi$ (with n an integer number). For this reason, the barrier is transparent when the condition

$$s'qL\cos\theta = n\pi \tag{51}$$

holds [20,21]. Therefore, for a fixed value of L there can be several θ values, and accordingly, ϕ values for which total transmission is expected, reaching a resonance condition. This can be observed in Fig. 4(a), (b) and (d), where T, R and R' as a function of ϕ are represented in the different energy zones.

The behavior of the transmission and reflection coefficients is shown in Fig. 4(a)–(d). In Fig. 4(a) we study the case $m = 0$, because of the interest in reproducing the case of graphene and other materials with Dirac-like quasiparticles. In Ref. [7], the transmission through an $L = 100$ nm wide barrier in a graphene system is considered, such that the parameters of charge carrier density outside (inside) the barrier are $n_1 = 0.5 \times 10^{12}$ cm^{-2} ($n_2 = -1 \times 10^{12}$ cm^{-2}). By knowing that the energy and potential of the quasiparticles is calculated as $E = \text{sign}(n_1)\sqrt{\pi\hbar^2 v_F^2 |n_1|}$, and $V_0 = E - \text{sign}(n_2)\sqrt{\pi\hbar^2 v_F^2 |n_2|}$, with $v_F = c/300$ the Fermi velocity, the energy and potential are $E = 82.44$ meV and $V_0 = 199$ meV. Translating this into dimensionless quantities normalized with respect to the energy, we obtain $V_0/E \approx 2.4$, and a dimensionless length parameter of value $EL/(\hbar v_F) \approx 12.5$, being those the values used for the plot in Fig. 4(a). It is observed that our transmission coefficient matches the one obtained for graphene in Ref. [7], and that perfect transmission is expected for normal incidence. Most importantly, it is observed that the reflection coefficient for inverted helicity states is always zero, meaning that the reflection and transmission process conserves the helicity of the massless fermions, even at arbitrary incidence angles.

Fig. 4(b) shows a similar situation as Fig. 4(a), but in the case of massive fermions. Here, the energy–mass ratio is $E/m = 2$, and the other parameters are $V_0/m = 4.8$ and $Lm = 6.25$, such that V_0/E and LE have the same values as in the massless case considered before. In the figure, graphene's massless case is represented by $T_{Katsnelson}$, with $V_0/E = 2.4$ and $EL = 12.5$. The most important conclusion is that the mass term implies a non-zero reflection coefficient for states with inverted helicity, specially at normal incidence where the reflection probability is entirely made out of it. It can be concluded that the mass term breaks the helicity conservation in the system, allowing the reflection of states with inverted helicity and limiting the transmission probability at normal incidence.

The analysis of the diffusion, evanescent and Klein energy zones applies to the potential barrier as well, because the momentum q_1 inside the barrier is still given by $q_1 = \sqrt{(E - V_0)^2 - m^2 - p_2^2}$. Fig. 4(a) and (b) represent the Klein energy zone, specially, the case where $V_0 > 2E$ where no transition to the evanescent zone is present.

Fig. 4(c) and (d) represent the diffusion and Klein zones, respectively. Since $V_0 < 2E$, a transition to the evanescent zone possible, as it is evident when noting zero transmission from some incidence angles. The critical angle analysis also applies for this system, however, it is noticed that T does not abruptly go to zero. Angles of total transmission also occur in those energy zones, and in a similar way as in the step potential, the reflection is dominated by inverted helicity states at small incidence angles, and by conserved helicity states at large ones.

Finally, we examine the behavior of the reflection and transmission coefficients in the massless case. In this limit we have that $P = s$ and $Q = s'$, thus Eqs. (47)–(49) change to

$$R = \frac{4\sin^2\beta\,|\sin\phi - \sin\theta|^2}{\left|2i\sin\beta - [e^{i\beta}\cos(\theta-\phi) + e^{-i\beta}\cos(\theta+\phi)]\right|^2}, \tag{52}$$

$$R' = 0, \tag{53}$$

$$T = \frac{4\cos^2\phi\cos^2\theta}{\left|2i\sin\beta - [e^{i\beta}\cos(\theta-\phi) + e^{-i\beta}\cos(\theta+\phi)]\right|^2}. \tag{54}$$

The reflection coefficient in Eq. (52) is equal to the one found by Katsnelson et al. for pristine graphene in Ref. [7], when using the natural units $\hbar = v_F = 1$. In that reference, the appearance of the band indices s and s' in the corresponding formula for the probability amplitude r (and in consequence, the reflection coefficient R) is explicit, while in ours it is not. This discrepancy is explained by the fact that the authors do not consider negative angles in their formulas, while in ours their sign depends on s and s', and with this consideration both results are equivalent in all scenarios. Fig. 4(a) shows the perfect agreement between them.

To end our discussion, we analyze the behavior of T as a function of V_0/E and m, for fixed values of L and ϕ. In Fig. 5(a) we show the normal incidence case, considering $LE = 12.5$ as in the previous examples, while the remaining quantities are normalized with respect to the energy. It is observed

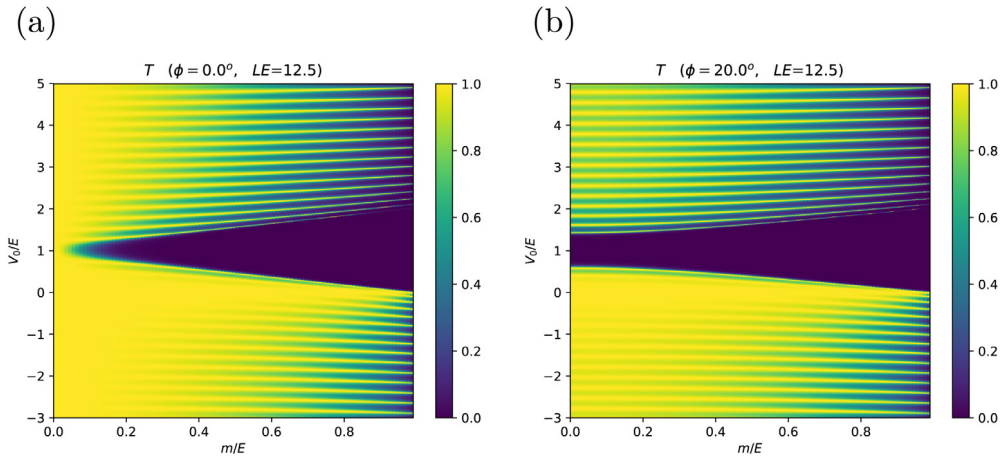

Fig. 5. Behavior of T for the barrier potential, for fixed LE and ϕ, as a function of m/E and V_0/E. As in Fig. 3, high to low transmission is plotted in yellow to blue colors, with dark blue representing zero transmission. (a) Transmission coefficient for conserved helicity states T at normal incidence, $\phi = 0$. At fixed m/E, it is observed the presence of regions with high and low transmission, consistent with the resonance condition in Eq. (51). (b) Transmission coefficient T at $\phi = 20°$. Absence of transmission around $V_0/E = 1$ corresponds to the transition of the system to the evanescent zone. (For interpretation of the references to color in this figure legend, the reader is referred to the web version of this article.)

that for fixed medium to high mass values, there is an oscillatory behavior of T, corresponding to the transmission resonance condition in Eq. (51). We have included negative values of the potential, which represent an electrostatic attractive potential for positive charged fermions, i.e. a potential well. Qualitatively, it can be seen that the behavior for negative V_0 is somewhat similar compared to a positive one, but overall there is higher transmission in the former case. In Fig. 5(b) the same situation is shown but for $\phi = 20°$, and as in the step potential, the region of zero transmission around $V_0/E = 1$ explained by the fact that the system is in the evanescent energy zone.

5. Conclusions

In this paper, we have presented the transmission and reflection coefficients for helicity conservation and inversion states, in step and barrier potentials, considering helicity-polarized incoming fermions. For the step potential, we have found that states with conserved helicity dominate the transmission if $V_0 < E$, however, as V_0 grows larger than E, the states with inverted helicity become dominant by roughly two orders of magnitude in most cases. We have also shown that at normal incidence, the reflection coefficient for conserved helicity is zero, even in the general case of massive fermions. This means that for low incidence angles, the reflection is dominated by states with inverted helicity. We have also discussed that this fact is important in graphene, because the reflection coefficient for helicity inversion is always zero, implying helicity conservation and total transmission at normal incidence. As a consequence, we have observed that the mass term breaks the helicity conservation, limiting the transmission in the system by allowing the reflection of inverted helicity states.

Additionally, by studying the behavior of the reflection and transmission in all the energy zones, we have found conditions for total reflection in step and barrier potentials. We have shown that if $0 < V_0 < 2E$, there exists an incidence angle from which total reflection is expected, marking the system's transition from the Klein or diffusion zone to the evanescent zone. The case $E - m \leq V_0 \leq E + m$ is most interesting, because total reflection happens independent of the angle of incidence. This fact can be used in the design of a filter in p-n junctures in graphene and Weyl semimetals, which can serve to collimate charge carriers in the device. In a different study, we have found that

this is linked to a conductance gap in p-n and n-p-n junctures of gapped graphene, and other solid state systems with massive Dirac-like charge carriers [27].

In the barrier potential, we have found that the transmission coefficient for helicity inversion states is always zero even in the case $V_0 > E$, in accordance to Refs. [20,21]. This implies that the helicity inversion process gets confined within the barrier, and the effect outside it is a total helicity conservation in the transmitted fermions, even if this is not the case for the reflected ones. Again, in the $m = 0$ limit the reflection coefficient for helicity inverted states is zero, and there is total transmission for normal incidence.

As was mentioned, the mass term breaks the helicity conservation, limiting the transmission in the system. This fact has important consequences in n-p-n junctures of graphene and Dirac materials, because Klein tunneling is an undesirable effect in a graphene-based transistor, since it implies that the device cannot be turned off, a fundamental feature of field effect transistors. In Ref. [27], we have applied the results obtained in this work to the study of the conductance in single-layer graphene and gapped single-layer graphene, where the charge carriers gain an effective mass. This has allowed us to describe the transport properties of such systems, finding that the effective mass opens up a conductance gap which depends quadratically on the bandgap [27].

Declaration of competing interest

The authors declare that they have no known competing financial interests or personal relationships that could have appeared to influence the work reported in this paper.

Appendix. Reflection and transmission amplitudes in the barrier potential

To solve the linear system of equations in Eqs. (36) and (37) and obtain the reflection and transmission amplitudes, the idea is to find a relation between the amplitudes r and r' with t and t', linked through the amplitudes a, a', b, and b'. From Eq. (37) it follows that

$$M_2 M_1^{-1} M_1 \begin{pmatrix} a \\ a' \\ b \\ b' \end{pmatrix} = V \begin{pmatrix} t \\ t' \end{pmatrix},$$
$$M_2 M_1^{-1} U \begin{pmatrix} 1 \\ r \\ r' \end{pmatrix} = V \begin{pmatrix} t \\ t' \end{pmatrix}. \tag{A.1}$$

Where the last equality is obtained from Eq. (36). It is straightforward to prove that M_1^{-1} is

$$M_1^{-1} = \frac{1}{4Q\cos\theta} \begin{pmatrix} Qe^{-i\theta} & s'Q & e^{-i\theta} & s' \\ -s'Q & Qe^{i\theta} & s' & -e^{i\theta} \\ Qe^{i\theta} & -s'Q & e^{i\theta} & -s' \\ s'Q & Qe^{-i\theta} & -s' & -e^{-i\theta} \end{pmatrix}. \tag{A.2}$$

Multiplying this matrix by M_2 on the left, it follows that

$$M_2 M_1^{-1} = \begin{pmatrix} G & 0 & 0 & \frac{H}{Q} \\ 0 & F & \frac{H}{Q} & 0 \\ 0 & QH & G & 0 \\ QH & 0 & 0 & F \end{pmatrix}, \tag{A.3}$$

where it has been defined

$$F = \frac{e^{i\beta}e^{i\theta} + e^{-i\beta}e^{-i\theta}}{2\cos\theta}, \tag{A.4}$$

$$G = \frac{e^{i\beta}e^{-i\theta} + e^{-i\beta}e^{i\theta}}{2\cos\theta}, \tag{A.5}$$

$$H = \frac{is'\sin\beta}{\cos\theta}. \tag{A.6}$$

Multiplying $M_2 M_1^{-1}$ with U on the left, Eq. (A.1) changes to

$$\begin{pmatrix} G + \frac{sP}{Q}He^{i\phi} & G - s\frac{P}{Q}He^{-i\phi} & sGe^{i\phi} + \frac{P}{Q}H \\ sFe^{i\phi} + \frac{P}{Q}H & -sFe^{-i\phi} + \frac{P}{Q}H & F - s\frac{P}{Q}He^{i\phi} \\ sQHe^{i\phi} + GP & -sQHe^{-i\phi} + PG & QH - sPGe^{i\phi} \\ QH + sFPe^{i\phi} & QH - sPFe^{-i\phi} & sQHe^{i\phi} - PF \end{pmatrix} \begin{pmatrix} 1 \\ r \\ r' \end{pmatrix}$$
$$= e^{i\alpha} \begin{pmatrix} 1 & -se^{-i\phi} \\ se^{i\phi} & 1 \\ P & sPe^{-i\phi} \\ sPe^{i\phi} & -P \end{pmatrix} \begin{pmatrix} t \\ t' \end{pmatrix}. \tag{A.7}$$

Finally, multiplying the first two rows of Eq. (A.7) by Q, and reorganizing the terms, we arrive at the following system of equations,

$$\begin{pmatrix} QG - sPHe^{-i\phi} & sQGe^{i\phi} - PH & -Qe^{i\alpha} & sQe^{-i\phi}e^{i\alpha} \\ -sQFe^{-i\phi} + PH & QF - sPHe^{i\phi} & -sQe^{i\phi}e^{i\alpha} & -Qe^{i\alpha} \\ -sQHe^{-i\phi} + PG & QH - sPGe^{i\phi} & -Pe^{i\alpha} & -sPe^{-i\phi}e^{i\alpha} \\ QH - sPFe^{-i\phi} & sQHe^{i\phi} - PF & -sPe^{i\phi}e^{i\alpha} & Pe^{i\alpha} \end{pmatrix} \begin{pmatrix} r \\ r' \\ t \\ t' \end{pmatrix}$$
$$= \begin{pmatrix} -QG - sPHe^{i\phi} \\ -sQFe^{i\phi} - PH \\ -sQHe^{i\phi} - PG \\ -QH - sPFe^{i\phi} \end{pmatrix}. \tag{A.8}$$

From which the reflection and transmission amplitudes in Eqs. (42)–(45) are obtained.

References

[1] O. Klein, Y. Nishina, Z. Phys. 52 (11–12) (1929) 853–868, http://dx.doi.org/10.1007/BF01366453.
[2] A. Calogeracos, N. Dombey, Internat. J. Modern Phys. A 14 (04) (1999) 631–643, http://dx.doi.org/10.1142/S0217751X99000312.
[3] F. Sauter, Z. Phys. 69 (11–12) (1931) 742–764, http://dx.doi.org/10.1007/BF01339461.
[4] A. Calogeracos, N. Dombey, Contemp. Phys. 40 (5) (1999) 313–321, http://dx.doi.org/10.1080/001075199181387.
[5] W. Greiner, B. Müller, J. Rafelski, Quantum Electrodynamics of Strong Fields, Springer, 1985.
[6] J. Schwinger, Phys. Rev. 82 (1951) 664, http://dx.doi.org/10.1103/PhysRev.82.664, URL https://link.aps.org/doi/10.1103/PhysRev.82.664.
[7] M.I. Katsnelson, K.S. Novoselov, A. Geim, Nat. Phys. 2 (2006) 620–625, http://dx.doi.org/10.1038/nphys384.
[8] A.H. Castro Neto, F. Guinea, N.M.R. Peres, K.S. Novoselov, A.K. Geim, Rev. Modern Phys. 81 (2009) 109–162, http://dx.doi.org/10.1103/RevModPhys.81.109.
[9] A.F. Young, P. Kim, Nat. Phys. 5 (2009) 222–226, http://dx.doi.org/10.1038/nphys1198.
[10] N. Stander, B. Huard, D. Goldhaber-Gordon, Phys. Rev. Lett. 102 (2009) 026807, http://dx.doi.org/10.1103/PhysRevLett.102.026807.
[11] S. Chen, Z. Han, M.M. Elahi, K.M.M. Habib, L. Wang, B. Wen, Y. Gao, T. Taniguchi, K. Watanabe, J. Hone, A.W. Ghosh, C.R. Dean, Science 353 (6307) (2016) 1522–1525, http://dx.doi.org/10.1126/science.aaf5481, URL http://www.ncbi.nlm.nih.gov/pubmed/27708099.
[12] V.H. Nguyen, J.-C. Charlier, Phys. Rev. B 97 (2018) 235113, http://dx.doi.org/10.1103/PhysRevB.97.235113, URL https://link.aps.org/doi/10.1103/PhysRevB.97.235113.
[13] Y. Xie, Y. Tan, A.W. Ghosh, Phys. Rev. B 96 (2017) 205151, http://dx.doi.org/10.1103/PhysRevB.96.205151, URL https://link.aps.org/doi/10.1103/PhysRevB.96.205151.
[14] K.M.M. Habib, R.N. Sajjad, A.W. Ghosh, Phys. Rev. Lett. 114 (2015) 176801, http://dx.doi.org/10.1103/PhysRevLett.114.176801, URL https://link.aps.org/doi/10.1103/PhysRevLett.114.176801.
[15] S. Li, A.V. Andreev, B.Z. Spivak, Phys. Rev. B 94 (8) (2016) 081408, http://dx.doi.org/10.1103/PhysRevB.94.081408, URL https://link.aps.org/doi/10.1103/PhysRevB.94.081408.
[16] F. Schwierz, Nature Nanotechnol. 5 (2010) 487, URL http://dx.doi.org/10.1038/nnano.2010.89.

[17] A. Varlet, M.-H. Liu, D. Bischoff, P. Simonet, T. Taniguchi, K. Watanabe, K. Richter, T. Ihn, K. Ensslin, Phys. Status Solidi (RRL) - Rapid Res. Lett. 10 (1) (2016) 46–57, http://dx.doi.org/10.1002/pssr.201510180, URL http://doi.wiley.com/10.1002/pssr.201510180.
[18] G. Giovannetti, P.A. Khomyakov, G. Brocks, P.J. Kelly, J. van den Brink, Phys. Rev. B 76 (2007) 073103, http://dx.doi.org/10.1103/PhysRevB.76.073103, URL https://link.aps.org/doi/10.1103/PhysRevB.76.073103.
[19] J. Sławińska, I. Zasada, Z. Klusek, Phys. Rev. B 81 (2010) 155433, http://dx.doi.org/10.1103/PhysRevB.81.155433, URL https://link.aps.org/doi/10.1103/PhysRevB.81.155433.
[20] S. De Leo, P. Rotelli, Phys. Rev. A 86 (2012) 032113, http://dx.doi.org/10.1103/PhysRevA.86.032113, URL https://link.aps.org/doi/10.1103/PhysRevA.86.032113.
[21] S. De Leo, P. Rotelli, Eur. Phys. J. C 63 (1) (2009) 157–162, http://dx.doi.org/10.1140/epjc/s10052-009-1060-9.
[22] M. Setare, D. Jahani, Physica B 405 (5) (2010) 1433–1436, http://dx.doi.org/10.1016/j.physb.2009.12.015.
[23] M.R. Setare, D. Jahani, J. Phys: Condens. Matter. 22 (2010) 245503, http://dx.doi.org/10.1088/0953-8984/22/24/245503.
[24] R.D.Y. Hills, F.V. Kusmartsev, Ann. Phys. 526 (9–10) (2014) 437–448, http://dx.doi.org/10.1002/andp.201400147, arXiv: https://onlinelibrary.wiley.com/doi/pdf/10.1002/andp.201400147.
[25] J. Viana Gomes, N.M.R. Peres, J. Phys.: Condens. Matter 20 (32) (2008) 325221, http://dx.doi.org/10.1088/0953-8984/20/32/325221, URL http://stacks.iop.org/0953-8984/20/i=32/a=325221?key=crossref.5ac075ac8373e6b94227b6fe1c7d0123.
[26] X.-G. Xu, C. Zhang, G.-J. Xu, J.-C. Cao, X. Xu-Guang, Z. Chao, X. Gong-Jie, C. Jun-Cheng, Chin. Phys. B 20 (2) (2011) 027201, http://dx.doi.org/10.1088/1674-1056/20/2/027201, URL http://stacks.iop.org/1674-1056/20/i=2/a=027201?key=crossref.de1b2450e7c15f17da0d0a952b511d59.
[27] J.A. Navarro-Giraldo, C.J. Quimbay, J. Phys.: Condens. Matter 30 (26) (2018) 265304, URL http://stacks.iop.org/0953-8984/30/i=26/a=265304.
[28] W. Greiner, Relativistic Quantum Mechanics: Wave Equations, third ed., Springer, 2000.
[29] V.G. Veselago, Sov. Phys. Usp. 10 (4) (1968) 509, URL http://stacks.iop.org/0038-5670/10/i=4/a=R04.
[30] V.V. Cheianov, V. Falko, B.L. Altshuler, Science 315 (5816) (2007) 1252–1255, http://dx.doi.org/10.1126/science.1138020, arXiv: http://science.sciencemag.org/content/315/5816/1252.full.pdf.
[31] P. Roushan, J. Seo, C.V. Parker, Y.S. Hor, D. Hsieh, D. Qian, A. Richardella, M.Z. Hasan, R.J. Cava, A. Yazdani, Nature 460 (2009) 1106, URL http://dx.doi.org/10.1038/nature08308.